





Short-timescale γ -Ray Variability in CTA 102

A. Shukla¹, K. Mannheim¹, S. R. Patel², J. Roy³ , V. R. Chitnis², D. Dorner¹, A. R. Rao⁴ , G. C. Anupama⁵, and C. Wendel¹¹Institute for Theoretical Physics and Astrophysics, Universität Würzburg, D-97074 Würzburg, Germany; amit.shukla@astro.uni-wuerzburg.de²Department of High Energy Physics, Tata Institute of Fundamental Research, Mumbai 400005, India³UM-DAE Center for Excellence in Basic Sciences, Mumbai 400098, India⁴Department of Astronomy and Astrophysics, Tata Institute of Fundamental Research, Mumbai 400005, India⁵Indian Institute of Astrophysics, Bangalore 560 034, India

Received 2017 November 29; revised 2018 January 21; accepted 2018 January 28; published 2018 February 16

Abstract

The flat-spectrum radio quasar CTA 102 experienced a prolonged state of enhanced activity across the entire observed electromagnetic spectrum during 2016–2017, most pronounced during a major outburst between 2016 December and 2017 May. *Fermi*-LAT observed a flux of $(2.2 \pm 0.2) \times 10^{-5}$ photons $\text{cm}^{-2} \text{s}^{-1}$ at energies above 100 MeV on 2017 April 19 during a single orbit. We report here the detection of significant (4.7σ) flux variations down to timescales of ~ 5 minutes during this orbit. The measured variability timescale is much shorter than the light-travel time across the central black hole (~ 70 minutes) indicating a very compact emission region within the jet, similar to that seen in IC 310, Mrk 501, or PKS 1222+21 from MAGIC observations. This short-timescale variability is unexpected since the γ -ray spectrum shows no sign of attenuation due to pair creation in interactions with photons from the broad emission line region, and therefore must be assumed to originate far from the black hole. The observed fast variability could either indicate the dissipation of magnetic islands or protons in a collimated beam from the base of the jet encountering the turbulent plasma at the end of the magnetic nozzle.

Key words: galaxies: active – galaxies: jets – gamma rays: galaxies – quasars: individual (CTA 102)

1. Introduction

The γ -ray emission of blazars is commonly assumed to be associated with shocks traveling down the jet or with the jet formation region near the central supermassive black hole (SMBH). Minute-scale and sub-hour-scale variability detected at γ -ray energies challenges this current paradigm for the location of the γ -ray emission. The shortest variability timescales found in PKS 2155-304, Mrk 501, and IC 310 (Aharonian et al. 2007; Albert et al. 2007; Aleksić et al. 2014) are shorter than the light-travel time across the event horizon, indicating very compact and anisotropic emission regions, plausibly occurring in the jet formation region. However, observations of short-term variability and changes in spectral behavior of flat-spectrum radio quasars (FSRQs) such as 3C 279 (Ackermann et al. 2016; Abdo et al. 2010), PKS 1222+216 (Aleksić et al. 2011), PMN J2345-1555 (Ghisellini et al. 2013), and PKS 1510-089 (Nalewajko et al. 2012) imply compact emission regions located far away from the SMBH and outside of the broad-line region (BLR) in order to avoid pair creation in γ -ray collisions with ambient low-energy photons (Lindfors et al. 2005). Observations of 3C 454.3 showed marginal evidence for the γ -ray emitting region to be located within the BLR (Isler et al. 2013; León-Tavares et al. 2013). By contrast, Jorstad et al. (2013) suggest the γ -ray emitting region to be outside of the BLR.

CTA 102 (B2230+114) is an FSRQ at a redshift of $z \sim 1.037$, well known for its high optical polarization ($>3\%$) and classified as a highly polarized quasar (Moore & Stockman 1981). Previous episodes of radio flares were found to be associated with the ejection of new knots from the core (Jorstad et al. 2005). Very Long Baseline Array images at 43 GHz, covering the time span from 2007 to 2014 June, suggested that the emitting region for optical and γ -ray photons should be >12 pc from the black hole (Casadio et al. 2015).

CTA 102 showed a few bright γ -ray flares during 2016–2017. During these flares, the *Fermi*-LAT detection of intra-day variability above 100 MeV allowed a study of the γ -ray emitting regions in FSRQs. We present a flux variability study of CTA 102 and its implications on the γ -ray emission mechanism during flaring activities.

2. *Fermi*-LAT Analysis

The pass8 *Fermi*-LAT γ -ray data⁶ (>100 MeV) of CTA 102 discussed in this work have been analyzed using the standard analysis procedure (Science Tools version v10r0p5) provided by the *Fermi*-LAT collaboration. A circular region of 10° radius was chosen around CTA 102 for the analysis. A zenith angle cut of 90° , the GTMKTIME cut of DATA_QUAL==1 && LAT_CONFIG==1 together with the LAT event class==128, and the LAT event type ==3 were used. Spectral analysis on the resulting data set was carried out by including *gll_iem_v06.fits* and the isotropic diffuse model *iso_PSR2_SOURCE_V6_v06.txt*. A power-law model was used to fit the energy spectrum of CTA 102, and its flux and spectrum were determined by using an unbinned glike algorithm based on the NewMinit optimizer (Cash 1979; Mattox et al. 1996).

3. Results

3.1. High Activity

CTA 102 was found to be in a prolonged outburst state in the entire electromagnetic spectrum during 2016 November to 2017 June, as reported in radio (INAF Medicina 32 m radio telescope; Righini et al. 2016), optical (Colgate University Foggy Bottom Observatory; Balonek et al. 2016), and high-energy γ -rays (*Fermi*-LAT, AGILE, and DAMPE; Ciprini 2016; Minervini et al. 2016; Xu et al. 2016). A major activity episode occurred in 2016

⁶ <https://fermi.gsfc.nasa.gov/ssc/data/>

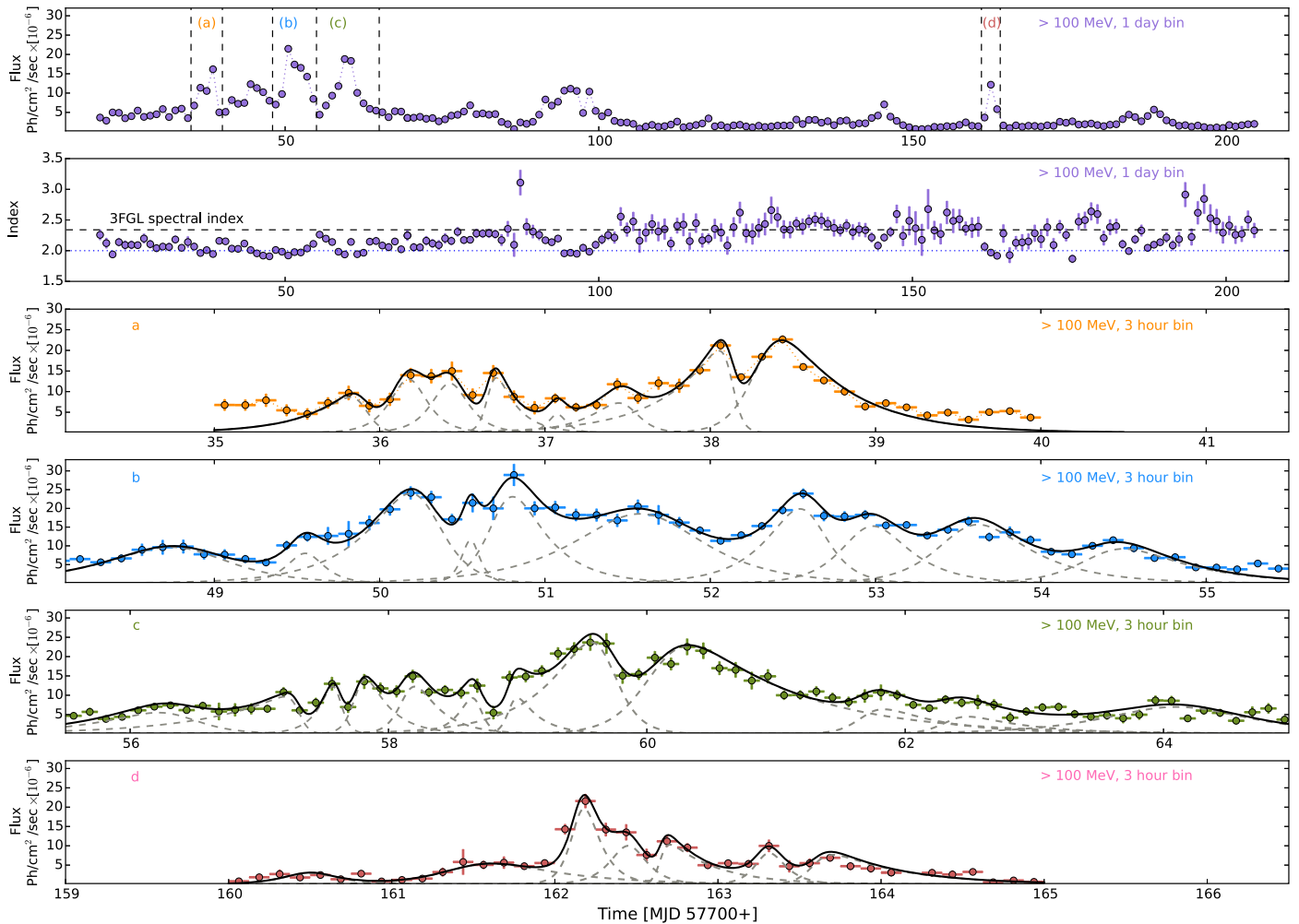


Figure 1. Light curve of CTA 102 over a six-month period is shown in the top panel (one-day binning). The corresponding power-law indices are presented in the second panel from the top. Four bright flares identified as “a,” “b,” “c,” and “d” and marked using dashed lines in the top panel are selected for a detailed study. The last four panels show zoomed three-hour binned light curves for these four flares. These have been fitted by a sum of exponentials in order to show the temporal evolution of the flux.

December that was followed by a few extremely bright flares and a very powerful GeV γ -ray outburst on 2017 April 19 (Ciprini 2017).

We have studied the source during this high activity period from 2016 December to 2017 May. The one-day binned light curve based on *Fermi*-LAT observations above 100 MeV, spanning this six-month period, is presented in Figure 1 (top panel). The corresponding spectral indices are shown in the second panel of Figure 1. The source spectrum was found to be very hard during these flares. Three-hour binned, zoomed light curves for the four bright flares, indicated as “a,” “b,” “c,” and “d” in the top panel of Figure 1, are shown in panels 3, 4, 5, and 6, respectively. These three-hour binned light curves have been fitted by a sum of exponentials in order to show the temporal evolution of the flux. The functional form of the fitted function is defined as

$$F(t) = 2F_0 \left[\exp\left(\frac{t_0 - t}{T_r}\right) + \exp\left(\frac{t - t_0}{T_d}\right) \right]^{-1}, \quad (1)$$

where F_0 is the flux at time t_0 representing the approximate flare amplitude, and T_r and T_d are the rise and decay times of the flare, respectively. To calculate the minimum flux doubling

time between the time instants t_1 and t_2 , each flare is scanned separately by using the following function:

$$F(t_2) = F(t_1) \cdot 2^{(t_2 - t_1)/t_d}. \quad (2)$$

$F(t_1)$ and $F(t_2)$, respectively, are the fluxes measured at t_1 and t_2 , and t_d represents the flux doubling timescale.

Several photon events with an energy above 20 GeV were observed during the active period. The highest-energy photon was observed during flare “a” (energy ~ 25 GeV). Another 24 GeV photon event was observed during flare “d.”

3.2. Sub-horizon Scale Variability

The four flaring events “a,” “b,” “c,” and “d” (see Figure 1) exhibit intra-day flux variations. In order to study this, the time binning is further refined up to good time intervals (gti) within each orbital period (which is ≤ 95 minutes). The fastest variability among these flares was observed during flare “d.” A doubling timescale of ~ 60 minutes in the observer frame is measured, starting from MJD 57861.898 to MJD 57862.030 in the orbit-binned light curve (Figure 2, top left panel). The second fastest variability was observed in flare “a” during MJD 57738 with a ~ 2 hr flux doubling timescale. The peak flux during flare “d” was observed during a ~ 40 minute stretch

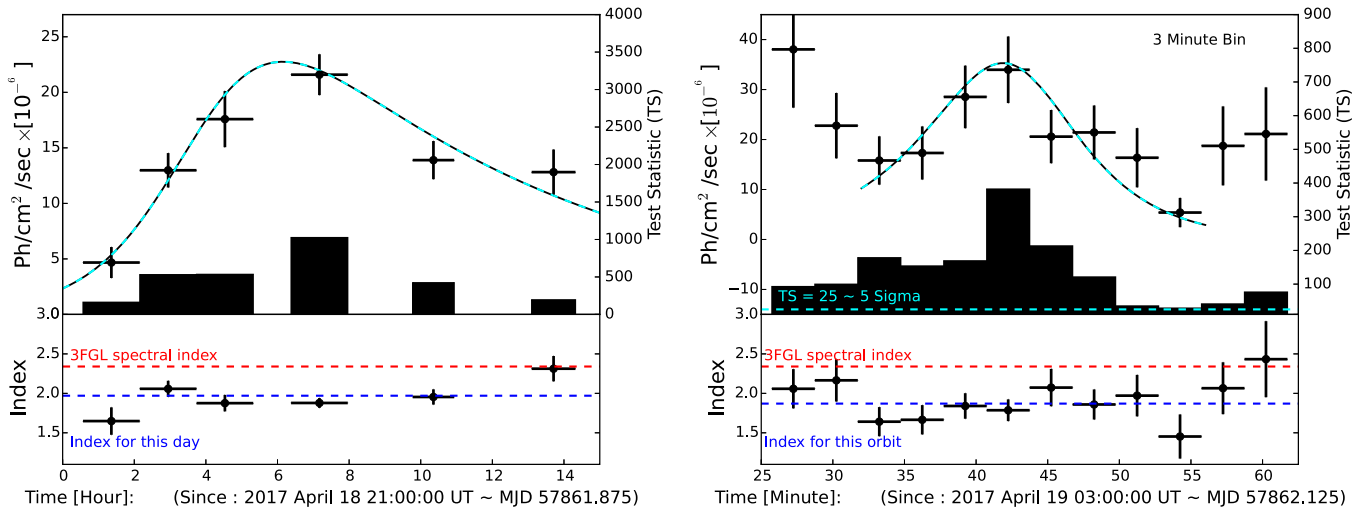


Figure 2. Left: the orbit-binned light curve of CTA 102 on 2017 April 19 is shown in the top panel with the TS values (black bars) plotted for each bin. The bottom panel shows the power-law index for each bin, the average power-law index of 2017 April 19 is plotted with a blue dashed line. Right: the top panel shows a three-minute binned light curve during an orbit where a strong hint of rapid variability is observed. The TS values (black bars) for each three-minute bin are plotted in the same panel and a cyan dashed line represents the 5σ detection. The bottom panel shows the power-law index as measured by *Fermi*-LAT for each three-minute bin during this flare. The average power-law index of this orbit is plotted with a blue dashed line. The red dashed line in both the bottom panels represents the value of the power-law index obtained from the 3FGL catalog. Both orbit-binned (gti) and three-minute binned light curves have been fitted by a sum of exponentials in order to show the temporal evolution using a cyan-black dashed line.

between MJD 57862.141 and MJD 57862.168. The integral flux above 100 MeV was found to be $(2.2 \pm 0.2) \times 10^{-5}$ photons $\text{cm}^{-2} \text{s}^{-1}$, which is ~ 150 times that of the 3FGL catalog flux value with test statistic (TS) ~ 1025 .

The very high flux during the flares provides an opportunity to probe ultra-fast variability with timescales of the order of a few minutes. A systematic search to detect ultra-fast variability during flares “a,” “b,” “c,” and “d” was carried out. The flux within each orbit is fitted with a constant flux, and the probability of the flux to be a constant is computed. The p -values in most of the orbits are found to be consistent with a constant flux except for two orbits. During these two orbits, the p -values are 0.17 (MJD 57738.534-57738.568) and 0.0011 (MJD 57862.141-57862.168), respectively, within the flares “a” and “d.” Ackermann et al. (2016) find a similar p -value in a single orbit during a rapid flare in 3C 279. The flux variability during the peak of flare “d,” with a p -value of 0.0011, has a significance of $\chi^2/\text{NDF} = 31/11$. A three-minute binned light curve (>100 MeV) of this orbit is shown in the top right panel of Figure 2. A flux doubling timescale of the order of ~ 4 minutes was observed with 2.7σ during the rise of the flare, and a flux halving timescale of the order of ~ 5 minutes was observed with 4.7σ during the decay of the flare in the observer’s frame. During this orbit, the source was found to be in a very hard spectral state with an index of 1.9 (see the bottom right panel of Figure 2). The peak flux observed during this orbit was $(3.3 \pm 0.6) \times 10^{-5}$ photons $\text{cm}^{-2} \text{s}^{-1}$ with a TS value of ~ 300 . The TS value for each three-minute bin is also shown in the top panel of Figure 2. The distributions of TS values and observed fluxes correlate strongly.

The distributions of the rise and decay times computed from Equation (1) are shown in Figure 3 for flares “a,” “b,” “c,” and “d” from the three-hour binned light curves. The thin and thick blue lines represent the size of event horizon for a maximally rotating and a spin zero black hole, respectively. The peaks of the distributions suggest that most of the variability observed is of the order of the event horizon timescale.

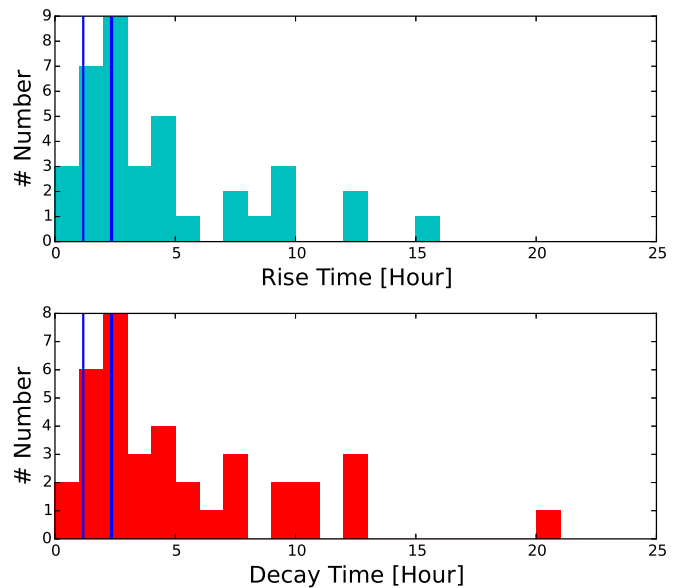


Figure 3. Distributions of the rise and decay times during all four flares based on the three-hour binned light curve computed from Equation (1). The thin and thick blue lines represent the size of the event horizon for a maximally rotating and a spin zero black hole, respectively, for CTA 102.

X-ray observations were carried out by *Swift*-XRT on 2017 April 20 during flare “d.” The data were analyzed using the standard procedures in the XRT data analysis software (XRTDAS⁷) distributed within HEASOFT⁸ version 6.19.

The source spectrum was fitted with an absorbed power law and was found to be hard with an index of 1.5 ± 0.04 . The integral flux between 0.3 and 8 keV was found to be $\sim 2 \times 10^{-11}$ erg $\text{cm}^{-2} \text{s}^{-1}$.

⁷ <http://www.asdc.asi.it/articles.php?id=26>

⁸ <https://heasarc.nasa.gov/lheasoft/>

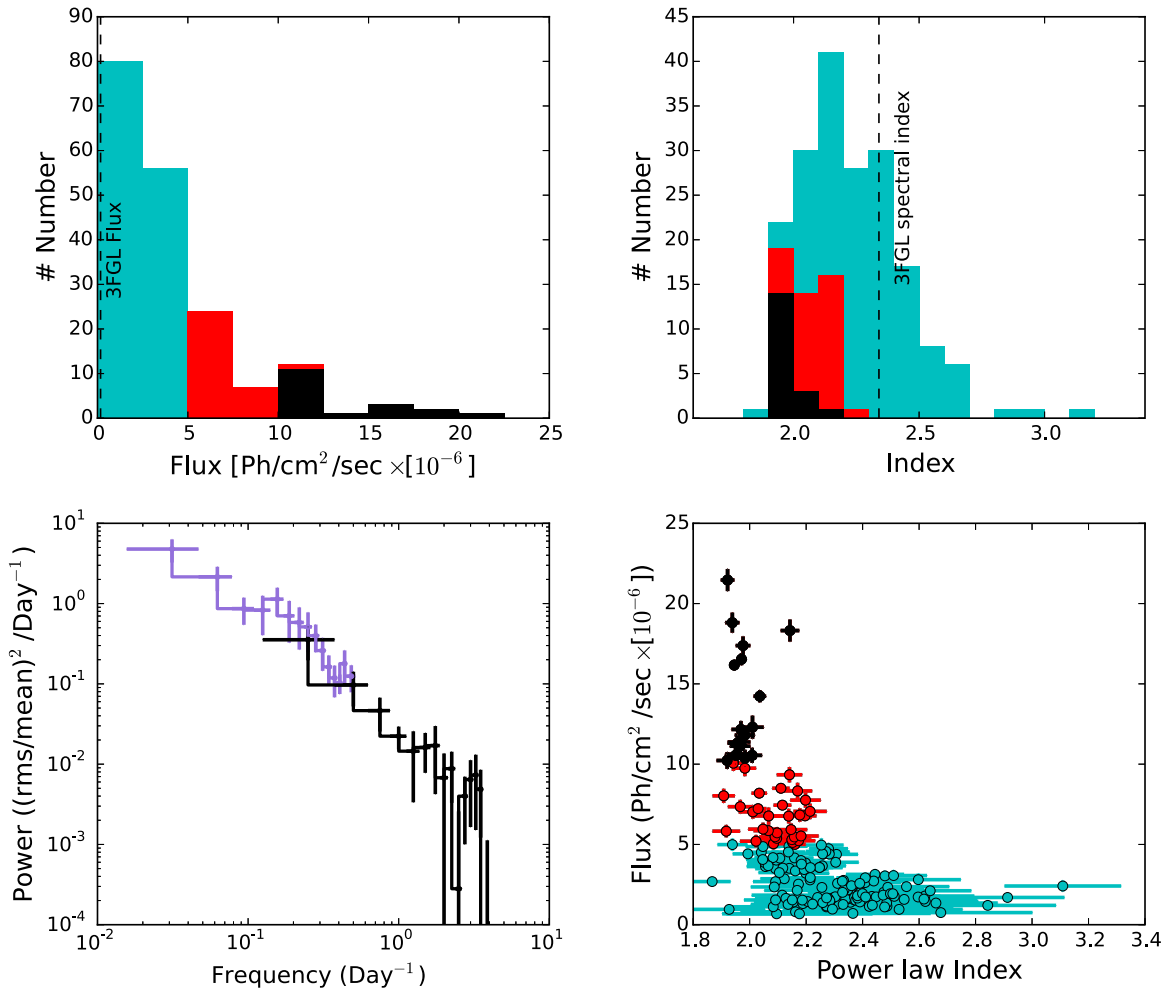


Figure 4. Flux distribution over the six-month period studied here is shown in the top left panel, and the corresponding power-law index distribution in the top right panel. The dashed black lines plotted in their respective panels are the 3FGL values for flux and power-law index for CTA 102, respectively. The indices corresponding to the fluxes are color coded; the index distribution shown in red and black corresponds to the flux distribution shown in the same color. The bottom left panel shows the PDS for the one-day (violet) and three-hour (black) binned light curves. The bottom right panel shows the flux vs. index plot, where the brighter when harder trend is clearly visible.

3.3. Power Density Spectrum

The available *Fermi*-LAT data allowed us to study the power density spectrum (PDS) on different timescales. Using the ftools task “powspec” in XRONOS,⁹ the PDS was generated for the one-day binned light curve and the three-hour binned light curve. The two PDS are shown in the bottom left panel of Figure 4. The light curves were divided into stretches of 32 bins per interval. PDSs from all segments were averaged to produce the final PDS for the observation. The white noise (Poissonian noise) subtracted PDS of the source exhibits a continuum that is best fitted by a power law of slope -1.6 in the frequency range 0.03 – 4 day $^{-1}$.

3.4. Spectrum

The spectra during this high activity were found to be significantly harder than those reported from this source in the 3FGL catalog (Acero et al. 2015). The flux and spectral index distributions during the six-month period are shown in the top left and the top right panels of Figure 4. The source shows a very significant hardening of the spectra during high flux. The

spectral indices for fluxes above 5×10^{-6} and 1×10^{-5} photons $\text{cm}^{-2} \text{s}^{-1}$ are also shown in the same figure in red and black, respectively. The measured spectral index above 100 MeV was found to be harder than 2 for most of the flux states with a flux above 1×10^{-5} photons $\text{cm}^{-2} \text{s}^{-1}$.

The spectra and indices of all major flares are found to be very similar and flat, respectively, as evident in Figure 5. The similarity in the spectral behavior for all these flares suggests that their origin might be similar. We have found no evidence for any absorption in the γ -ray spectra. If the emission originates inside the BLR then γ -rays should suffer pair creation due to interactions with Thomson scattered light from the accretion flow or with recombination lines, in which case the γ -ray spectrum should show a break around a few GeV (Poutanen & Stern 2010).

The optical spectra from the SPOL CCD Imaging/Spectropolarimeter at Steward Observatory (Smith et al. 2009) were used to study the behavior of the Mg line during the high state. We did not find any conclusive correlation between the Mg line flux and the continuum flux, a similar conclusion is also drawn by Bachev et al. (2017). However, during the high state, the Mg line is not visible and the spectrum is dominated by the continuum emission.

⁹ <https://heasarc.gsfc.nasa.gov/xanadu/xronos/xronos.html>

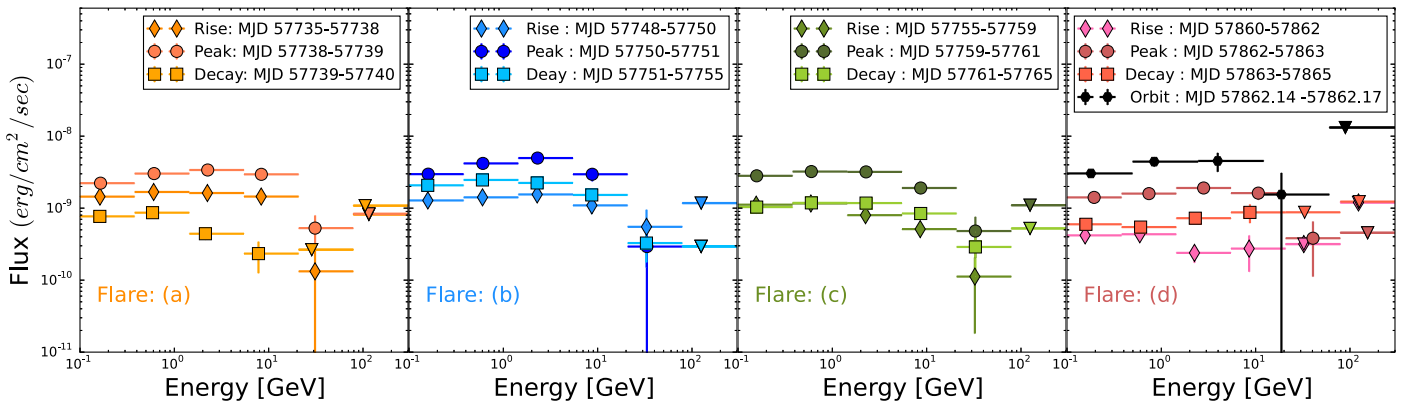


Figure 5. *Fermi*-LAT SEDs are shown during their rise (diamonds), peak (circles), and decay (squares) of the four flares. The black dots in the fourth panel represent the *Fermi*-LAT SED during the orbit that has the highest flux within flare “d.” Triangles represent an upper limit in the plots.

4. Discussion

CTA 102 harbors an SMBH with a mass of $8.5 \times 10^8 M_{\odot}$ (Zamaninasab et al. 2014), which corresponds to an event horizon light-crossing time of ~ 70 minutes for a maximally rotating black hole. The detection of fast variability of the order of a few minutes suggests a very compact emission region of the radius $R' \sim \delta \cdot 10^{13} / (1 + z)$ cm. Emission from such compact region is very difficult to reconcile with the far-dissipation scenarios, if the emission is produced across the entire jet area.

The detection of high-energy photons > 20 GeV during the flares puts constraints on the location of the γ -ray emission region in CTA 102. Liu & Bai (2006) computed the γ -ray optical depth as a function of the location of the γ -ray emitting region, and they found that the BLR is opaque for γ -rays above $20 \text{ GeV} / (1 + z)$, if the emitting source is located within the BLR. This is due to the interaction of the γ -rays mainly with H-Ly $_{\alpha}$ and continuum emission for FSRQs with an accretion disk luminosity above $10^{45} \text{ erg s}^{-1}$. For CTA 102, an optical depth $\tau_{\gamma\gamma} > 1$ for γ -ray photons of various energies was also found assuming a spherical geometry by Pacciani et al. (2014), concluding that it is unlikely that the emission above ~ 10 GeV originates within a BLR of radius $R_{\text{BLR}} \sim 6.4 \times 10^{17}$ cm. The minimum Doppler factor computed from the γ - γ transparency argument considering an X-ray flux of $2 \times 10^{-11} \text{ erg cm}^{-2} \text{ s}^{-1}$ is found to be $\delta \sim 25$.

The γ -ray flux reaches nearly $10^{-9} \text{ erg cm}^{-2} \text{ s}^{-1}$, corresponding to an apparent γ -ray luminosity of $\sim 10^{49} \text{ ergs s}^{-1}$. The brightest fluxes observed from CTA 102 during this active period are comparable to previously observed bright flares from 3C 279 (Hayashida et al. 2015) and 3C 454.3 (Abdo et al. 2011). CTA 102 becomes the third and farthest FSRQ to show variability of the order of a few minutes timescale after 3C 279 (Ackermann et al. 2016) and PKS 1222+216 (Aleksić et al. 2011).

4.1. Magnetic Islands

In order to explain this compact emission region with a radius smaller than the jet radius, we consider magnetic islands traveling down the jet and becoming unstable outside the BLR (cf. Giannios et al. 2009). It is envisaged that a fraction of the magnetic energy released by the ergosphere or disk surrounding the SMBH occasionally dissipates through the X-point magnetic reconnection at the base of the jet (close to the event horizon; Nodes et al. 2003). Thereby created magnetic loops may survive traveling down the jet in its magnetically

dominated regime up to ~ 0.1 pc (a similar phenomenon is observed in the solar wind scenario; Sheeley et al. 1997; Einaudi et al. 2001; Eriksson et al. 2014; Sanchez-Diaz et al. 2017). We propose that the observed fast variability indicates the dissipation of these magnetic islands, carrying a certain fraction of the Eddington luminosity, when they encounter the turbulent plasma at the end of the magnetic nozzle where jet collimation breaks down and the jet becomes dominated by the kinetic energy of its particle inventory.

The high energy density of the emission region requires magnetic islands to be formed in regions with Eddington-strength magnetic fields close to the black hole. Indeed, high-resolution observations of a nearby radio jet provide evidence for Eddington magnetic field strengths ($B' \sim 10^4$ G) at the base of the jet (Baczko et al. 2016).

Considering a magnetic island of a co-moving frame with a radius of $R' \sim 10^{14}$ cm and a Doppler factor $\delta \sim 25$ that carries 10% ($\eta = 0.1$) of the Eddington luminosity to the assumed turbulent region, and which is then converted with an efficiency of 10% ($\zeta = 0.1$) into photon luminosity, the total photon luminosity L_{ph} in the observer’s frame is

$$L_{\text{ph}} = \eta \left(\frac{B'^2}{8\pi} \right) \cdot \pi r'^2 c \zeta \delta^4 \text{ erg s}^{-1} \quad (3)$$

$$\sim 1.5 \times 10^{49} \text{ erg s}^{-1}, \quad (4)$$

which is close to the actual observed γ -ray luminosity in the energy band 0.1 – 300 GeV $\sim 2.3 \times 10^{49} \text{ erg s}^{-1}$ during the rapid flare.

It is conceivable that several of these magnetic islands were launched from the base of the jet during the high activity of CTA 102 resulting in the superimposed light curve as observed during 2016 December and 2017 January, which did not allow us to detect fast variability during this period. However, during 2017 April, we might have observed the emission from a single distinct magnetic island reflected by the fast variability. The magnetic island scenario also helps to produce a strong Compton hump outside the BLR as a significant amount of magnetic energy is transferred to particles in the emission zone. The mass loading of the decaying islands might be the result of pair production by high-energy photons with a high multiplicity. Mini-jets resulting from the dissipation of the magnetic islands would lead to shocks and subsequent 1st order Fermi acceleration (Drake et al. 2006). As particles are shock accelerated in sequence with the blob decay, we will expect a

harder-when-brighter trend from the source. We additionally expect multi-wavelength correlations, since first-order Fermi acceleration produces very broad energy distributions.

4.2. Proton Beam



Another option to interpret the fast variability is by considering a hadronic scenario. Collimated proton beams may originate as a result of electric fields induced by a rotating SMBH surrounded by an accretion disk with a poloidal magnetic field (Lovelace 1976). The anomalous resistivity due to turbulence at the edge of the BLR leads to the disruption of the proton beam (Lesch et al. 2002). Electrons accelerated in this turbulent region (Norman & Ter Haar 1975) produce synchrotron photons acting as a target for the relativistic protons (Mannheim & Biermann 1992). The resulting photo-meson decay initiates electromagnetic cascades and neutrino emission. The brightest *Fermi*-LAT flares have neutrino detection probabilities of the order of a few percent in IceCube (Kadler et al. 2016). So far, no event coincident with CTA 102 has been reported by IceCube.

5. Summary

In this Letter, we report sub-horizon-scale γ -ray variability as measured by *Fermi*-LAT in the FSRQ CTA 102. *Fermi*-LAT measured ~ 5 minutes halving time with 4.7σ confidence on 2017 April 19. The observed rapid variability challenges the standard SSC or EC scenarios. We propose that magnetic islands produced by explosive X-point reconnection at the base of the jet, and subsequently traveling down the jet, could leave the BLR to dissipate their energy into relativistic particles, giving rise to the observed flux variations. Alternatively, proton beams could transport the energy to larger distances from the central SMBH, leading to cascade emission when the beam is disrupted by plasma instabilities.

This research has also made use of data obtained from the High Energy Astrophysics Science Archive Research Center (HEASARC), provided by NASA's Goddard Space Flight Center. Data from the Steward Observatory spectropolarimetric monitoring project were used. This program is supported by Fermi Guest Investigator grants NNX08AW56G and NNX09AU10G. A.S. thanks Prof. P. Subramanian for a fruitful discussion. The support by BMBF Verbundforschung FKZ 05A17WW1 is acknowledged.

ORCID iDs

J. Roy  <https://orcid.org/0000-0002-2329-5863>
A. R. Rao  <https://orcid.org/0000-0003-0833-0533>

References

- Abdo, A. A., Ackermann, M., Ajello, M., et al. 2010, *Natur*, **463**, 919
 Abdo, A. A., Ackermann, M., Ajello, M., et al. 2011, *ApJL*, **733**, L26
 Acero, F., Ackermann, M., Ajello, M., et al. 2015, *ApJS*, **218**, 23
 Ackermann, M., Anantua, R., Asano, K., et al. 2016, *ApJL*, **824**, L20
 Aharonian, F., Akhperjanian, A. G., Bazer-Bachi, A. R., et al. 2007, *ApJL*, **664**, L71
 Albert, J., Aliu, E., Anderhub, H., et al. 2007, *ApJ*, **669**, 862
 Aleksić, J., Ansoldi, S., Antonelli, L. A., et al. 2014, *Sci*, **346**, 1080
 Aleksić, J., Antonelli, L. A., Antoranz, P., et al. 2011, *ApJL*, **730**, L8
 Bachev, R., Popov, V., Strigachev, A., et al. 2017, *MNRAS*, **471**, 2216
 Baczko, A.-K., Schulz, R., Kadler, M., et al. 2016, *A&A*, **593**, A47
 Balonek, T. J., Zhang, S., Chapman, K. J., et al. 2016, *ATel*, **9732**
 Casadio, C., Gómez, J. L., Jorstad, S. G., et al. 2015, *ApJ*, **813**, 51
 Cash, W. 1979, *ApJ*, **228**, 939
 Ciprini, S. 2016, *ATel*, **9869**
 Ciprini, S. 2017, *ATel*, **10292**
 Drake, J. F., Swisdak, M., Che, H., & Shay, M. A. 2006, *Natur*, **443**, 553
 Einaudi, G., Chibbaro, S., Dahlburg, R. B., & Velli, M. 2001, *ApJ*, **547**, 1167
 Eriksson, S., Newman, D. L., Lapenta, G., & Angelopoulos, V. 2014, *PPCF*, **56**, 064008
 Ghisellini, G., Tavecchio, F., Foschini, L., Bonnoli, G., & Tagliaferri, G. 2013, *MNRAS*, **432**, L66
 Giannios, D., Uzdensky, D. A., & Begelman, M. C. 2009, *MNRAS*, **395**, L29
 Hayashida, M., Nalewajko, K., Madejski, G. M., et al. 2015, *ApJ*, **807**, 79
 Isler, J. C., Urry, C. M., Coppi, P., et al. 2013, *ApJ*, **779**, 100
 Jorstad, S. G., Marscher, A. P., Lister, M. L., et al. 2005, *AJ*, **130**, 1418
 Jorstad, S. G., Marscher, A. P., Smith, P. S., et al. 2013, *ApJ*, **773**, 147
 Kadler, M., Krauß, F., Mannheim, K., et al. 2016, *NatPh*, **12**, 807
 León-Tavares, J., Chavushyan, V., Patiño-Álvarez, V., et al. 2013, *ApJL*, **763**, L36
 Lesch, H., Birk, G. T., & Schopper, R. 2002, *PPCF*, **44**, 1
 Lindfors, E. J., Valtaoja, E., & Türler, M. 2005, *A&A*, **440**, 845
 Liu, H. T., & Bai, J. M. 2006, *ApJ*, **653**, 1089
 Lovelace, R. V. E. 1976, *Natur*, **262**, 649
 Mannheim, K., & Biermann, P. L. 1992, *A&A*, **253**, L21
 Mattox, J. R., Bertsch, D. L., Chiang, J., et al. 1996, *ApJ*, **461**, 396
 Minervini, G., Piano, G., Munar-Adrover, P., et al. 2016, *ATel*, **9743**
 Moore, R. L., & Stockman, H. S. 1981, *ApJ*, **243**, 60
 Nalewajko, K., Sikora, M., Madejski, G. M., et al. 2012, *ApJ*, **760**, 69
 Nodes, C., Birk, G. T., Lesch, H., & Schopper, R. 2003, *PhPI*, **10**, 835
 Norman, C. A., & Ter Haar, D. 1975, *PhLC*, **17**, 308
 Pacciani, L., Tavecchio, F., Donnarumma, I., et al. 2014, *ApJ*, **790**, 45
 Poutanen, J., & Stern, B. 2010, *ApJL*, **717**, L118
 Righini, S., Giroletti, M., D'Ammando, F., et al. 2016, *ATel*, **9884**
 Sanchez-Diaz, E., Rouillard, A. P., Davies, J. A., et al. 2017, *ApJL*, **835**, L7
 Sheeley, N. R., Wang, Y.-M., Hawley, S. H., et al. 1997, *ApJ*, **484**, 472
 Smith, P. S., Montiel, E., Rightley, S., et al. 2009, arXiv:0912.3621
 Xu, Z.-L., Caragiulo, M., Chang, J., et al. 2016, *ATel*, **9901**
 Zamaninasab, M., Clausen-Brown, E., Savolainen, T., & Tchekhovskoy, A. 2014, *Natur*, **510**, 126